





# Correlating electron trapping and structural defects in Al<sub>2</sub>O<sub>3</sub> thin films deposited by plasma enhanced atomic layer deposition

Cite as: AIP Advances **10**, 125017 (2020); <https://doi.org/10.1063/5.0023735>

Submitted: 31 July 2020 . Accepted: 20 November 2020 . Published Online: 11 December 2020

 Emanuela Schilirò,  Patrick Fiorenza, Corrado Bongiorno, Corrado Spinella, Salvatore Di Franco,   
Giuseppe Greco, Raffaella Lo Nigro, and  Fabrizio Roccaforte

## COLLECTIONS

Paper published as part of the special topic on [Chemical Physics](#), [Energy, Fluids and Plasmas](#), [Materials Science](#) and [Mathematical Physics](#)



View Online



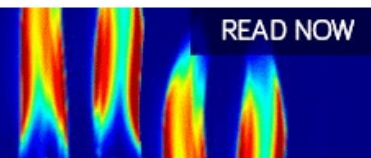
Export Citation



CrossMark

AIP Advances  
Fluids and Plasmas Collection

READ NOW



# Correlating electron trapping and structural defects in Al<sub>2</sub>O<sub>3</sub> thin films deposited by plasma enhanced atomic layer deposition

Cite as: AIP Advances 10, 125017 (2020); doi: 10.1063/5.0023735

Submitted: 31 July 2020 • Accepted: 20 November 2020 •

Published Online: 11 December 2020







View Online



Export Citation



CrossMark

Emanuela Schilirò,  Patrick Fiorenza,<sup>a)</sup>  Corrado Bongiorno, Corrado Spinella, Salvatore Di Franco, Giuseppe Greco,  Raffaella Lo Nigro, and Fabrizio Roccaforte 

## AFFILIATIONS

Consiglio Nazionale delle Ricerche, Istituto per la Microelettronica e Microsistemi (CNR-IMM), Strada VIII, 5 Zona Industriale, 95121 Catania, Italy

<sup>a)</sup> Author to whom correspondence should be addressed: [patrick.fiorenza@imm.cnr.it](mailto:patrick.fiorenza@imm.cnr.it)

## ABSTRACT

In this article, electron trapping in aluminum oxide (Al<sub>2</sub>O<sub>3</sub>) thin films grown by plasma enhanced atomic layer deposition on AlGaIn/GaN heterostructures has been studied and a correlation with the presence of oxygen defects in the film has been provided. Capacitance–voltage measurements revealed the occurrence of a negative charge trapping effect upon bias stress, able to fill an amount of charge traps in the bulk Al<sub>2</sub>O<sub>3</sub> in the order of  $5 \times 10^{12} \text{ cm}^{-2}$ . A structural analysis based on electron energy-loss spectroscopy demonstrated the presence of low-coordinated Al cations in the Al<sub>2</sub>O<sub>3</sub> film, which is an indication of oxygen vacancies, and can explain the electrical behavior of the film. These charge trapping effects were used for achieving thermally stable (up to 100 °C) enhancement mode operation in AlGaIn/GaN transistors, by controlling the two-dimensional electron gas depletion.

© 2020 Author(s). All article content, except where otherwise noted, is licensed under a Creative Commons Attribution (CC BY) license (<http://creativecommons.org/licenses/by/4.0/>). <https://doi.org/10.1063/5.0023735>

## INTRODUCTION

Aluminum oxide (Al<sub>2</sub>O<sub>3</sub>) is an attractive material for a variety of applications in electronic devices.<sup>1</sup> As an example, thin Al<sub>2</sub>O<sub>3</sub> layers can be used as a gate insulator to reduce the leakage current in gallium nitride (GaN) high electron mobility transistors (HEMTs) or as a passivation layer to reduce the current collapse phenomena in these devices.<sup>2,3</sup> The great interest toward Al<sub>2</sub>O<sub>3</sub> in the GaN technology arises from the excellent physical properties of this insulator, i.e., high dielectric constant  $\kappa$  (~9), high critical electric field (10 MV/cm), large bandgap (~8.9), and favorable band alignment with GaN.<sup>4</sup>

In this context, atomic layer deposition (ALD) is the most widely used technique today to deposit Al<sub>2</sub>O<sub>3</sub> thin films on GaN. In fact, ALD is a self-limited growth mechanism, enabling an accurate control of thickness and interface abruptness, and a uniform coverage at low deposition temperatures, i.e., compatible with the GaN thermal stability range and typical device processing.

In general, the quality of amorphous thin films grown by ALD can be extremely variable.<sup>5</sup> In particular, theoretical calculations show that Al<sub>2</sub>O<sub>3</sub> layers are characterized by the presence of native defects<sup>6–8</sup> that can also influence their electrical behavior (i.e., leakage current) by introducing electronic levels in the dielectric bandgap.<sup>9,10</sup>

In the last decade, the vast majority of the literature on GaN-based devices focused on the electrical behavior of thermal ALD Al<sub>2</sub>O<sub>3</sub> films.<sup>2–4,11–13</sup> Despite in some cases charge trapping phenomena have been observed, which lead to an instability of the Al<sub>2</sub>O<sub>3</sub>/AlGaIn device characteristics,<sup>11,13</sup> a clear correlation of these effects with the structural quality of the film has not been reported.

In this context, plasma enhanced atomic layer deposition (PE-ALD) is a promising alternative to the standard thermal ALD approach, possessing the advantage of higher growth rate and film density and low deposition temperature.<sup>14,15</sup> However, the origin of charge trapping at interface states and bulk oxide traps in PE-ALD Al<sub>2</sub>O<sub>3</sub> films on GaN-based heterostructures remains under

discussion,<sup>16,17</sup> thus hindering the full technological exploitation of these films.

In this paper, the electron trapping phenomena in Al<sub>2</sub>O<sub>3</sub> thin films deposited by plasma enhanced atomic layer deposition on AlGaIn/GaN heterostructures have been investigated and correlated with the interface and bulk structural quality of the film. In particular, the correlation of capacitance measurements upon stress and structural analyses allowed us to attribute the observed electron trapping to the presence of low-coordinated Al cations, i.e., oxygen vacancies in the Al<sub>2</sub>O<sub>3</sub> film. A practical implication of this physical effect on the insulated gate AlGaIn/GaN HEMT technology has been discussed, opening the possibility to fabricate thermally stable enhancement mode transistors.

## EXPERIMENTAL

Al<sub>2</sub>O<sub>3</sub> films have been deposited by Plasma Enhanced ALD (PE-ALD) onto AlGaIn/GaN heterostructures grown on Si(111) substrates. Prior to the Al<sub>2</sub>O<sub>3</sub> deposition, the AlGaIn surface has been treated by a sequential cleaning process using piranha (H<sub>2</sub>O<sub>2</sub>:H<sub>2</sub>SO<sub>4</sub> = 1:5) and diluted hydrofluoric acid (H<sub>2</sub>O:HF = 10:1) solutions, for 10 min and 5 min, respectively, in order to remove the carbon contamination and native oxide.<sup>18</sup> These chemical treatments, before the deposition process, were selected among different possibilities, which were explored in earlier research and whose effects on the electrical properties were evaluated.<sup>19</sup> The Al<sub>2</sub>O<sub>3</sub> deposition has been carried out on a PE-ALD LL reactor from SENTECH Instruments GmbH, using trimethyl-aluminum (TMA) and O<sub>2</sub>-plasma as aluminum and oxygen sources, respectively. The O<sub>2</sub>-plasma has been generated by a capacitively coupled plasma (CCP) source, through a 13.56 MHz RF-generator with a power of 200 W. For the plasma run, a 100 sccm O<sub>2</sub> flow was released to the plasma source. Nitrogen (N<sub>2</sub>) gas, with a flow rate of 40 sccm, has been used as a carrier for the TMA precursor. During the ALD cycle, pulse periods of 60 ms and 1 s for TMA and O<sub>2</sub>-plasma, respectively, have been coupled with the purging pulse of N<sub>2</sub> gas for 2 s. The deposition process has been carried out at 250 °C, with a chamber pressure of 20 Pa. According to the nominal growth rate of 1.2 Å/cycle, the number of cycles was chosen to be 250 in order to obtain an Al<sub>2</sub>O<sub>3</sub> film thickness of about 30 nm.

Circular Al<sub>2</sub>O<sub>3</sub>/AlGaIn/GaN metal–insulator–semiconductor (MIS) capacitors were fabricated to monitor the electrical quality of the bulk oxide and of the interface by capacitance–voltage (C–V) measurements under different bias stress conditions. In these control devices, the Ohmic contact was formed by an annealed Ti/Al/Ni/Au multilayer,<sup>20</sup> while the gate contact consisted of a Ni/Au bilayer.

Morphological, structural, and chemical analyses of the deposited Al<sub>2</sub>O<sub>3</sub> films were carried out employing a variety of techniques on blanket Al<sub>2</sub>O<sub>3</sub>/AlGaIn/GaN samples. In particular, atomic force microscopy (AFM) was carried out to investigate the surface morphology of the films, using a Veeco Dimension 3100 AFM with a NanoScope V controller. High-resolution transmission electron microscopy (HR-TEM) on cross-section samples enabled us to evaluate the film thickness as well as microstructural properties of the Al<sub>2</sub>O<sub>3</sub>/AlGaIn interface. The chemical nature of the Al<sub>2</sub>O<sub>3</sub> thin films was investigated by Electron Energy-Loss Spectroscopy (EELS) in the scanning transmission electron microscopy (STEM) mode with

a nanometer electron probe. Both kinds of analyses were carried out using a Field Emission Gun-TEM JEOL 2010F microscope.

Finally, Al<sub>2</sub>O<sub>3</sub>/AlGaIn/GaN metal–insulator–semiconductor high electron mobility transistors (MISHEMTs) have been fabricated and characterized by current–voltage (I–V) measurements, monitoring the stability of the transfer characteristics at high temperatures (up to 100 °C). The C–V and I–V measurements on capacitors and transistors were carried out using a Microtech Cascade probe station equipped with a Keysight B1505 parameter analyzer.

## RESULTS AND DISCUSSION

The growth of the Al<sub>2</sub>O<sub>3</sub> insulating layer on AlGaIn/GaN heterostructures has been obtained by the PE-ALD procedure described in detail elsewhere.<sup>19</sup> The role of surface preparation before deposition has been fully exploited, and the effects on the formation of interface defects have already been discussed in previously reported papers.<sup>17–19</sup> Here, the dielectric properties and charge trapping phenomena of Al<sub>2</sub>O<sub>3</sub> layers, grown by the PE-ALD optimized procedure,<sup>18,19</sup> have been investigated on Al<sub>2</sub>O<sub>3</sub>/AlGaIn/GaN MIS capacitors, by the C–V measurements, as reported in Fig. 1(a). These measurements have been carried out by sweeping the gate bias from negative toward positive values and backward. Different C–V curves have been sequentially collected by increasing the final gate bias value from 0 V to +15 V on “fresh” (non-stressed) MIS capacitors, and the hysteresis between the forward and backward C–V curves has been determined for each stress condition. In particular, these measurements allowed us to discriminate among the different trapping contributions at the Al<sub>2</sub>O<sub>3</sub>/AlGaIn and AlGaIn/GaN interfaces. It should be underlined that the sweeping rate did not affect the value of the hysteresis. The reported C–V curves have been acquired at 0.05 V/s, and each point has been averaged with four measurements. The first C–V measurement [the blue curve in Fig. 1(a)], collected from V<sub>G</sub> = −10 V to 0 V and backward, shows no hysteresis. The depletion of the two-dimensional electron gas (2DEG)<sup>21</sup> at the AlGaIn/GaN interface is clearly visible with a “pinch-off” of the curves at V<sub>PO</sub> = −7.5 V. The absence of hysteresis demonstrates that no charge trapping occurs by stressing the MIS capacitor in the negative gate bias range, i.e., at the AlGaIn/GaN interface where the 2DEG is located.

Furthermore, C–V curves have been collected by increasing the final positive gate bias stress up to +10 and +15 V [red and black curves in Fig. 1(a)]. Summarizing, the gate stress is applied by extending the V<sub>G</sub> bias toward larger positive values. Hence, initially, all the C–V measurements have been carried out at the gate bias ranging from −10 V to 0 V and backward, and then, the final bias value has been progressively increased up to +15 V. Under these conditions, the C–V curves first rise at the “flat band voltage” V<sub>FB</sub> and then exhibit a second step due to the accumulation of electrons in the AlGaIn layer at the Al<sub>2</sub>O<sub>3</sub> interface.

The C–V curves exhibit two capacitance saturation levels that correspond to the capacitance of the Al<sub>2</sub>O<sub>3</sub> layer (at a high positive gate bias) and to the series capacitance of the Al<sub>2</sub>O<sub>3</sub> and AlGaIn layer (in the V<sub>G</sub> range of −5 V/+5 V). Hence, from the accumulation capacitance, the relative permittivity of the Al<sub>2</sub>O<sub>3</sub> layer has been determined to be  $\kappa_{\text{Al}_2\text{O}_3} = 8.4$ , which is close to the theoretical Al<sub>2</sub>O<sub>3</sub> bulk value ( $\approx 9$ ), thus demonstrating the good dielectric quality of deposited films.

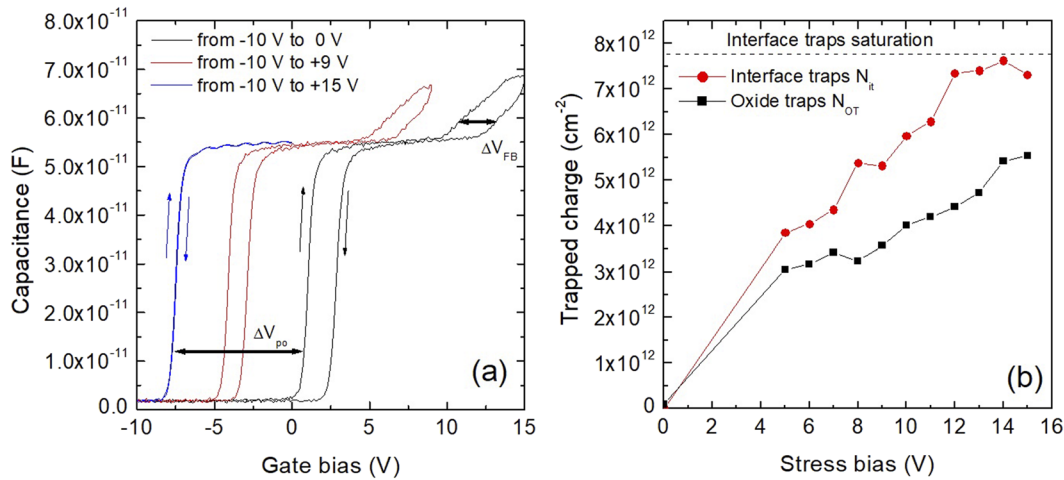


**FIG. 1.** (a) C–V curves collected on a MIS capacitor sweeping the gate bias from depletion-to-accumulation and backward, by increasing the value of the final gate bias. (b) Total amount of the Al<sub>2</sub>O<sub>3</sub>/AlGa<sub>N</sub> interface trapped charge and bulk oxide (Al<sub>2</sub>O<sub>3</sub>) trapped charge as a function of the positive gate bias stress. The values have been extracted from the C–V curves from the shifts  $\Delta V_{FB}$  and  $\Delta V_{PO}$ .

It is interesting to note that the hysteresis of the C–V curves is always observed under positive bias stress conditions, such as close to the pinch-off  $V_{PO}$  and to the flat band voltage  $V_{FB}$ . These hystereses can be associated with different charge trapping effects occurring in the MIS system.

To quantify these effects, the flat band voltage and pinch-off voltage shifts ( $\Delta V_{FB}$  and  $\Delta V_{PO}$ ) have been monitored as a function of the positive gate bias stress. In particular, these shifts are associated with the charging of the Al<sub>2</sub>O<sub>3</sub>/AlGa<sub>N</sub> interface states ( $\Delta V_{FB}$ ) and of the traps in the bulk Al<sub>2</sub>O<sub>3</sub> ( $\Delta V_{PO}$ ).<sup>22</sup> In fact, to provide a quantitative description of the observed charge trapping effects, the following assumptions are needed: (i) the insulator bulk traps are located at the Al<sub>2</sub>O<sub>3</sub>/AlGa<sub>N</sub> interface, as often described in the text books,<sup>23</sup> and are responsible for the shift of  $V_{PO}$  ( $\Delta V_{PO}$ ) in the C–V curves and (ii) the interface traps at the Al<sub>2</sub>O<sub>3</sub>/AlGa<sub>N</sub> interface are completely de-trapped under the application of negative  $V_G$  values.

Following the planar capacitor approximation, the total amount of charge trapped at the Al<sub>2</sub>O<sub>3</sub>/AlGa<sub>N</sub> interface ( $N_{it}$ ) can be obtained by

$$N_{it} = \frac{\Delta V_{FB} C_{Al_2O_3}}{q}, \quad (1)$$

where  $C_{Al_2O_3}$  is the insulator layer capacitance in accumulation and  $q$  is the electron charge.

Based on these assumptions, the capacitance plateau  $C_{PO}$  observed close to  $V_G = 0$  V are the series of the insulator ( $C_{Al_2O_3}$ ) and AlGa<sub>N</sub> layer ( $C_{AlGaN}$ ) capacitances,

$$C_{PO} = \left( \frac{1}{C_{Al_2O_3}} + \frac{1}{C_{AlGaN}} \right)^{-1}, \quad (2)$$

and are related to the  $V_{PO}$  shift ( $\Delta V_{PO}$ ) through the following equation [Eq. (3)]:

$$C_{PO} = \left( \frac{1}{C_{Al_2O_3}} + \frac{1}{C_{AlGaN}} \right)^{-1} = \frac{\Delta Q}{\Delta V} \equiv \frac{qN_{OT}}{\Delta V_{PO}}, \quad (3)$$

which has been used to calculate the total amount of trapped charges in the Al<sub>2</sub>O<sub>3</sub> film ( $N_{OT}$ ),

$$N_{OT} = \frac{\Delta V_{PO} \left( \frac{t_{Al_2O_3}}{\kappa_{Al_2O_3} \epsilon_0} + \frac{t_{AlGaN}}{\kappa_{AlGaN} \epsilon_0} \right)^{-1}}{q}, \quad (4)$$

where  $t_{Al_2O_3}$  and  $t_{AlGaN}$  are the Al<sub>2</sub>O<sub>3</sub> and AlGa<sub>N</sub> layer thicknesses, while  $\kappa_{Al_2O_3}$  and  $\kappa_{AlGaN}$  are the Al<sub>2</sub>O<sub>3</sub> and AlGa<sub>N</sub> relative permittivities.

Figure 1(b) reports the total amount of the trapped charges at the Al<sub>2</sub>O<sub>3</sub>/AlGa<sub>N</sub> interface ( $N_{it}$ ) and in the bulk Al<sub>2</sub>O<sub>3</sub> ( $N_{OT}$ ) as a function of the positive gate bias stress. The values have been extracted from the C/V curves from the shifts  $\Delta V_{FB}$  and  $\Delta V_{PO}$ , using Eqs. (1) and (4), respectively.

As can be seen, the value of  $N_{it}$  increases with the increase in the final positive bias stress value, until a saturation is observed at high stress bias, corresponding to a maximum of the trapped charge,  $N_{it} = 7 \times 10^{12} \text{ cm}^{-2}$ . In fact, by increasing the positive bias stress, in the MIS capacitor, on the AlGa<sub>N</sub>/Ga<sub>N</sub> heterostructure, electrons are spilled-over from the 2DEG and reach the Al<sub>2</sub>O<sub>3</sub>/AlGa<sub>N</sub> interface, where they can fill the available free traps until reaching saturation. Once the gate bias is swept backward, the Al<sub>2</sub>O<sub>3</sub>/AlGa<sub>N</sub> interface states are fully discharged.

On the other hand, the total amount of trapped charges in the bulk Al<sub>2</sub>O<sub>3</sub> does not show such a saturation with the increase in the bias stress [Fig. 1(b)]. The occurrence of a positive  $\Delta V_{PO}$  shift in the C–V curves is associated with the presence of slow traps in Al<sub>2</sub>O<sub>3</sub>, which retains the negative charge even after strong negative backward gate biasing. Hence, the positive shift occurs from the initial value (non-stressed MIS capacitor) and the  $\Delta V_{PO}$  in Eq. (2) is calculated from that initial  $V_{PO}$  value [see Fig. 1(a)]. In this case,

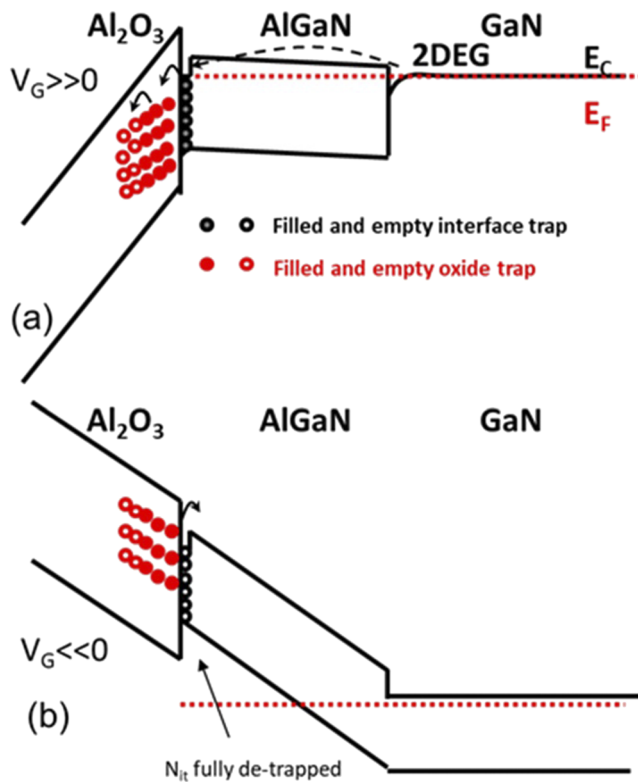


**FIG. 2.** Schematic energy band diagram of the  $\text{Al}_2\text{O}_3/\text{AlGaN}/\text{GaN}$  system at different gate bias regimes: (a)  $V_G \gg 0$  V, filling the interface and oxide traps with electrons, and (b)  $V_G \ll 0$  V, the discharging process of the interface traps and oxide traps.

the maximum of the  $\Delta V_{\text{PO}}$  shift measured after a +15 V stress corresponds to a maximum of  $N_{\text{OT}} = 5 \times 10^{12} \text{ cm}^{-2}$ .

The charge trapping/detrapping phenomena occurring in our system are graphically reported in Fig. 2, which shows a schematic band diagram of the  $\text{Al}_2\text{O}_3/\text{AlGaN}/\text{GaN}$  MIS system.

In particular, when the MIS capacitor is in accumulation ( $V_G \gg 0$ ), the electrons at the  $\text{Al}_2\text{O}_3/\text{AlGaN}$  interface can also fill the oxide traps inside the insulator layer ( $N_{\text{OT}}$ ). Once the capacitor is biased in the opposite direction ( $V_G \ll 0$ ), the interface traps are discharged, but the oxide traps retain their charged state. In fact, electrons in bulk oxide traps located near the oxide/nitride interfaces can be retained during reverse bias sweeps due to their long detrapping time even at high temperatures.<sup>17</sup>

The charge trapping phenomena observed in the C/V measurements have been correlated with the morphological and structural properties of the  $\text{Al}_2\text{O}_3$  films.

The surface morphology of the deposited  $\text{Al}_2\text{O}_3$  layers has been monitored by using an AFM [Fig. 3(a)] and is characterized by the presence of nanometric rounded grains. The root mean square roughness (RMS) of the film is 0.52 nm, i.e., only slightly higher compared to that of the AlGaN substrate (RMS = 0.32 nm). This latter indicates that the conformal coverage of the AlGaN surface has been achieved.

Then, TEM analysis has been carried out to assess the structural properties of the deposited  $\text{Al}_2\text{O}_3$  layer and to image its interface with the AlGaN substrate. In particular, the high resolution cross-sectional image (HR-TEM), shown in Fig. 3(b), revealed the formation of an amorphous and uniform layer of  $\text{Al}_2\text{O}_3$  having a thickness of about 30 nm, with an abrupt  $\text{Al}_2\text{O}_3/\text{AlGaN}$  interface and no evidence of an interfacial layer.<sup>24</sup> The good interface quality demonstrates the effectiveness of the surface treatment adopted prior to the PE-ALD and the absence of damage due to the remote plasma.

Further information on the microstructure of the  $\text{Al}_2\text{O}_3$  film has been gained by the STEM-EELS technique. In particular, Energy Loss Near-Edge Structure (ELNES) investigation has been performed on the sample, focusing on the Al  $L_{2-3}$ -edge whose shape is related to Al coordination.<sup>25</sup> In order to have a proper interpretation of the data, the Al  $L_{2-3}$ -edge acquired on the PE-ALD deposited  $\text{Al}_2\text{O}_3$  film has been compared to those of the tabulated defect-free crystalline phases ( $\alpha$ -,  $\gamma$ -)  $\text{Al}_2\text{O}_3$  with known Al-coordination [Fig. 3(c)].<sup>25</sup> The tabulated spectrum of the Al  $L_{2-3}$  edge in the  $\alpha$ - $\text{Al}_2\text{O}_3$  phase [Fig. 3(c), black line], consisting of only octahedrally coordinated Al cations (i.e., six O-coordinated Al), is identified by a high intensity peak centered at 79 eV and a much less intense peak at 80 eV.<sup>25,26</sup> On the other hand, the tabulated Al  $L_{2-3}$  edge of the  $\gamma$ - $\text{Al}_2\text{O}_3$  phase [Fig. 3(c), red line], consisting of both tetrahedrally (four-coordinated) and octahedrally coordinated Al cations, shows two signals at 78 eV and 79.5 eV, with inverted intensity compared to  $\alpha$ - $\text{Al}_2\text{O}_3$ .<sup>25-27</sup> For both  $\alpha$ -phase and  $\gamma$ -phase, the broad peak at about 84 eV is an indication of a medium-range crystalline structure. The experimental spectrum of the Al  $L_{2-3}$  edge obtained on our PE-ALD deposited  $\text{Al}_2\text{O}_3$  film [Fig. 3(c), green line] shows the absence of the peak at 84 eV due to the lack of the medium range order.<sup>28</sup> Moreover, it exhibits a split broad peak at about 79 eV and 78 eV, having the shape and energy position intermediate between the  $\alpha$ - and  $\gamma$ -phase and a second low-energy signal at 76.7 eV. All the features of this edge structure can be related either to the coexistence of four- and six-coordinated aluminum or also to other coordinated aluminum cations (3-, 5-) and, consequently, to the presence of distorted bonds.<sup>25,28-30</sup> The presence of low-coordinated aluminum cations, revealed by our analysis, can be associated with an inherent oxygen deficiency in the  $\text{Al}_2\text{O}_3$  film. In fact, *ab initio* calculations on low-coordinated aluminum atoms have indicated the presence of transition energy levels in the bandgap of the insulator, which can act as electron traps in the  $\text{Al}_2\text{O}_3/\text{AlGaN}$  system.<sup>6</sup>

It is well-known that, besides oxygen vacancies, also other defects, such as residual H and/or C species, could act as charge trapping centers within the dielectric material.<sup>31</sup> For this reason, the quantitative comparison between the experimental density of trapped charges and the amount of oxygen vacancies can be useful. From the  $\Delta V_{\text{PO}}$  of the C-V curves, the amount of trapped charges in the  $\text{Al}_2\text{O}_3$  of  $N_{\text{OT}} = 6 \times 10^{12} \text{ cm}^{-2}$  has been estimated. Assuming the filling of all the bulk traps in the  $\text{Al}_2\text{O}_3$  layer, their volume concentration (for a thickness of 30 nm) results to be about  $2 \times 10^{18} \text{ cm}^{-3}$ . In a more realistic scenario, under our bias stress conditions, electron trapping occurs in a limited portion of the insulator, i.e., within about 1 nm from the semiconductor interface, thus resulting in a volume trap charge density of about  $6 \times 10^{19} \text{ cm}^{-3}$ . Unfortunately, the quantification of the oxygen vacancies in



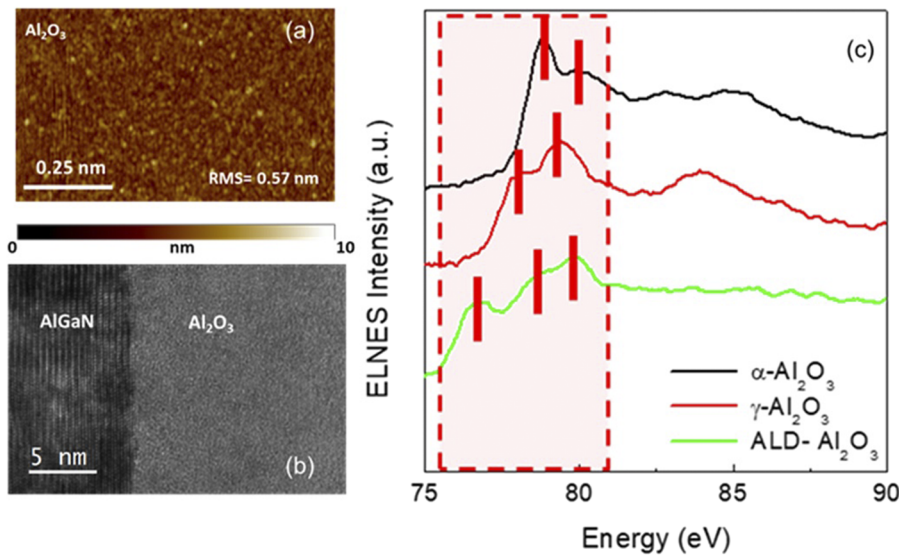


**FIG. 3.** (a) Morphological map acquired by using an AFM on the  $1 \times 1 \mu\text{m}^2$  areas of the PE-ALD  $\text{Al}_2\text{O}_3$  thin film. (b) High resolution cross-sectional TEM image of the  $\text{Al}_2\text{O}_3/\text{AlGaN}$  interface. (c) Energy loss near-edge structure (ELNES) spectra of the Al  $L_{2-3}$ -edge for the tabulated  $\alpha\text{-Al}_2\text{O}_3$  (black line) and  $\gamma\text{-Al}_2\text{O}_3$  (red line) and PE-ALD  $\text{Al}_2\text{O}_3$  thin films (green line).

amorphous  $\text{Al}_2\text{O}_3$  thin films only by our ELNES spectrum is not straightforward, as it would require standard amorphous  $\text{Al}_2\text{O}_3$  samples with a known oxygen vacancy content, which are not easily available. In fact, as proposed in the literature for other materials, such a quantification is done mainly by fitting the EELS spectra using theoretical calculations of the amorphous supercell with an appropriate amount of oxygen vacancies.<sup>32,33</sup> The electronic properties of oxygen vacancies in amorphous  $\text{Al}_2\text{O}_3$  have been discussed in the literature.<sup>9,34</sup> Perevalov *et al.* estimated an oxygen vacancy content for amorphous  $\text{Al}_2\text{O}_3$  thin films grown by ALD in the order of  $7 \times 10^{20} \text{ cm}^{-3}$ .<sup>7</sup> Based on the above considerations, since the experimental trapped charge density is lower than the expected oxygen

vacancy density, it is plausible to argue that not all these intrinsic defects are electrically active in our system.

Based on the above considerations, since the experimental trapped charge density is lower than the expected oxygen vacancy density, it is plausible to argue that not all these intrinsic defects are electrically active in our system.

Moreover, the presence of negative charges trapped inside the bulk  $\text{Al}_2\text{O}_3$  gate insulator can induce Coulombic screening of the underlying 2DEG at the AlGaN/GaN interface. Hence, it can be, in principle, used to achieve the enhancement mode operation in AlGaN/GaN HEMT devices, provided that the amount of negative charges trapped in the oxide is of the same order of magnitude of

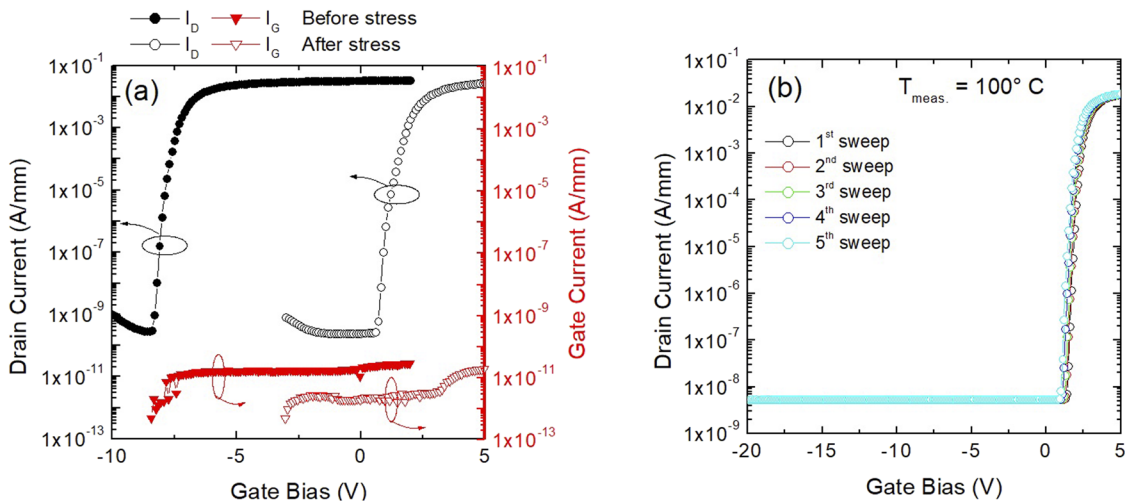


**FIG. 4.** (a) Transfer  $I_D$ - $V_G$  characteristics collected at  $V_{DS} = 0.1 \text{ V}$  for the  $\text{Al}_2\text{O}_3/\text{AlGaN}/\text{GaN}$  MISHEMT before (solid symbols) and after (open symbols) charge trapping by a positive gate bias at  $15 \text{ V}$ . The values of the gate current  $I_G$  are also shown by red symbols. (b) Series of five  $I_D$ - $V_G$  curves (stress at  $V_G = -20 \text{ V}$ ) sequentially collected at  $100^\circ\text{C}$ , showing the stability of enhancement mode operation.

the 2DEG density. The achievement of enhancement mode operation in AlGaIn/GaN HEMTs remains one of the most critical aspect in the GaN technology for future power electronics applications.<sup>35</sup>

Figure 4(a) reports the transfer characteristics ( $I_D$ - $V_G$ ) of the Al<sub>2</sub>O<sub>3</sub>/AlGaIn/GaN MISHEMT before and after a 15 V positive gate bias. As can be seen, after the positive gate bias, the MISHEMT shows an enhancement mode behavior, with a positive pinch-off bias  $V_{PO} = 1.3$  V. At the same time, the transistor still exhibits a low gate leakage current ( $I_G \sim 2 \times 10^{-11}$  A/mm at  $V_G = +5$  V). Johnson *et al.*<sup>22</sup> and Hou *et al.*<sup>36</sup> observed an analogous trapping effect in HfO<sub>2</sub> and Al<sub>2</sub>O<sub>3</sub> AlGaIn/GaN MISHEMTs and attributed it to the presence of a GaON interfacial layer formed during the thermal ALD process. However, in our PE-ALD film, the abrupt interface showed by HR-TEM analysis [Fig. 3(b)] confirms that the electrical behavior is ruled by the presence of structural defects within the Al<sub>2</sub>O<sub>3</sub> layer acting as charge traps. Those traps, in turn, seem to have no significant effect on the leakage current.

It is important to point out that the effect of the trapped charges in the Al<sub>2</sub>O<sub>3</sub> is stable with the temperature. In fact, Fig. 4(b) reports a sequence of five transfer characteristics of the device collected at 100 °C between  $V_G = -20$  V and +5 V. Evidently, these curves are completely overlapped, thus demonstrating the stability of the film to retain the trapped charge under high temperature operation that requires several days to be relaxed toward the initial condition.

Certainly, the thermal stability of the charge trapping in the bulk traps deserves to be fine controlled in order to achieve fully reliable enhancement mode AlGaIn/GaN HEMTs.

## CONCLUSIONS

In summary, electron trapping occurring in Al<sub>2</sub>O<sub>3</sub> films grown by plasma enhanced atomic layer deposition on AlGaIn/GaN heterostructures has been monitored and correlated with the structural properties of the films. In particular, C-V analyses allowed us to monitor the trapping/detrapping effects both in the bulk Al<sub>2</sub>O<sub>3</sub> and at the interface, providing an amount of Al<sub>2</sub>O<sub>3</sub> bulk traps in the order of  $N_{OT} = 5 \times 10^{12}$  cm<sup>-2</sup>. These defects can be filled with electrons under appropriate positive bias conditions. The ELNES spectra of the aluminum L<sub>2-3</sub>-edge demonstrated the occurrence of locally low coordinated aluminum cations in Al<sub>2</sub>O<sub>3</sub>, which are associated with an oxygen deficiency in the film. The local oxygen deficiency can be correlated with the presence of the electron traps in the insulator and can explain the electrical results. This charge trapping phenomenon can be intentionally used to control the depletion of the 2DEG at an AlGaIn/GaN interface, obtaining an enhancement mode operation stable up to 100 °C. Hence, the results can be particularly useful for device manufacturers and open new routes for achieving enhancement mode AlGaIn/GaN HEMTs.

## ACKNOWLEDGMENTS

The authors would like to thank F. Giannazzo (CNR-IMM) for the stimulating scientific discussions. This work was partially funded by the Italian Ministry for Education, University and Research (MIUR) in the framework of the National Project PON EleGaNTe (Electronics on GaN-based Technologies), Grant No. ARS01\_01007.

## DATA AVAILABILITY

The data that support the findings of this study are available from the corresponding author upon reasonable request.

## REFERENCES

- G. D. Wilk, R. M. Wallace, and J. M. Anthony, *J. Appl. Phys.* **89**, 5243–5275 (2001).
- F. Roccaforte, P. Fiorenza, G. Greco, M. Vivona, R. Lo Nigro, F. Giannazzo, A. Patti, and M. Saggio, *Appl. Surf. Sci.* **301**, 9–18 (2014).
- T. Hashizume, K. Nishiguchi, S. Kaneki, J. Kuzmik, and Z. Yatabe, *Mater. Sci. Semicond. Process.* **78**, 85–95 (2018).
- F. Roccaforte, P. Fiorenza, R. Lo Nigro, F. Giannazzo, and G. Greco, *Riv. Nuovo Cimento* **41**, 625–681 (2018).
- S.-J. Park, J.-P. Lee, J. S. Jang, H. Rhu, H. Yu, B. Y. You, C. S. Kim, K. J. Kim, Y. J. Cho, S. Baik, and W. Lee, *Nanotechnology* **24**, 295202 (2013).
- M. Choi, A. Janotti, and C. G. Van de Walle, *J. Appl. Phys.* **113**, 044501 (2013).
- T. V. Perevalov, O. E. Tereshenko, V. A. Gritsenko, V. A. Pustovarov, A. P. Yeliseyev, C. Park, J. H. Han, and C. Lee, *J. Appl. Phys.* **108**, 013501 (2010).
- J. Robertson, *Solid-State Electron.* **49**, 283–293 (2005).
- D. Liu, S. J. Clark, and J. Robertson, *Appl. Phys. Lett.* **96**, 032905 (2010).
- J. R. Weber, A. Janotti, and C. G. Van de Walle, *J. Appl. Phys.* **109**, 033715 (2011).
- S. Ganguly, J. Verma, G. Li, T. Zimmermann, H. Xing, and D. Jena, *Appl. Phys. Lett.* **99**, 193504 (2011).
- M. Esposito, S. Krishnamoorthy, D. N. Nath, S. Bajaj, T.-H. Hung, and S. Rajan, *Appl. Phys. Lett.* **99**, 133503 (2011).
- Y. Zhang, M. Sun, S. J. Joglekar, T. Fujishima, and T. Palacios, *Appl. Phys. Lett.* **103**, 033524 (2013).
- H. Kim and I.-K. Oh, *Jpn. J. Appl. Phys.* **53**, 03DA01 (2014).
- D. R. Boris, V. D. Wheeler, N. Nepal, S. B. Qadri, S. G. Walton, and C. R. Eddy, *J. Vac. Sci. Technol., A* **38**, 040801 (2020).
- M. Tapajna, L. Valik, F. Guemann, D. Gregusova, K. Froehlich, S. Hascik, E. Dobrocka, L. Tothand, B. Pecz, and J. Kuzmik, *J. Vac. Sci. Technol., B* **35**, 01A107 (2017).
- P. Fiorenza, G. Greco, E. Schilirò, F. Iucolano, R. Lo Nigro, and F. Roccaforte, *Jpn. J. Appl. Phys.* **57**, 050307 (2018).
- E. Schilirò, G. Greco, P. Fiorenza, C. Tudisco, G. G. Condorelli, S. Di Franco, F. Roccaforte, and R. Lo Nigro, *Phys. Status Solidi C* **12**, 980–984 (2015).
- R. Lo Nigro, E. Schilirò, G. Greco, P. Fiorenza, and F. Roccaforte, *Thin Solid Films* **617**, 138 (2016).
- G. Greco, F. Iucolano, and F. Roccaforte, *Appl. Surf. Sci.* **383**, 324–345 (2016).
- O. Ambacher, J. Smart, J. R. Shealy, N. G. Weimann, K. Chu, M. Murphy, W. J. Schaff, L. F. Eastman, R. Dimitrov, L. Wittmer, M. Stutzmann, W. Rieger, and J. Hilsenbeck, *J. Appl. Phys.* **85**, 3222–3233 (1999).
- D. W. Johnson, R. T. P. Lee, R. J. W. Hill, M. H. Wong, G. Bersuker, E. L. Piner, P. D. Kirsch, and H. R. Harris, *IEEE Trans. Electron Devices* **60**, 3197–3203 (2013).
- D. K. Schroder, *Semiconductor Material and Device Characterization*, 3rd ed. (Wiley, Hoboken, NJ, 2006).
- Q. Wang, X. Cheng, L. Zheng, L. Shen, J. Li, D. Zhang, R. Qian, and Y. Yu, *RSC Adv.* **7**, 11745–11751 (2017).
- D. Bouchet and C. Colliex, *Ultramicroscopy* **96**, 139–150 (2003).
- A. S. Konashuk, A. A. Sokolov, V. E. Drozd, F. Schaefer, and E. O. Filatova, *Thin Solid Films* **534**, 363–366 (2013).
- K. Kimoto, Y. Matsui, T. Nabatame, T. Yasuda, T. Mizoguchi, I. Tanaka, and A. Toriumi, *Appl. Phys. Lett.* **83**, 4306–4308 (2003).
- S. Fritz, A. Seiler, L. Radtke, R. Schneider, M. Weides, G. Weiß, and D. Gerthsen, *Sci. Rep.* **8**, 7956 (2018).
- L. Zeng, D. T. Tran, C.-W. Tai, G. Svensson, and E. Olsson, *Sci. Rep.* **6**, 29679 (2016).
- S. B. Lee, Y.-M. Kim, and H. N. Han, *AIP Adv.* **5**, 077181 (2015).

<sup>31</sup>M. Uenuma, K. Takahashi, S. Sonehara, Y. Tominaga, Y. Fujimoto, Y. Ishikawa, and Y. Uraoka, *AIP Adv.* **8**, 105103 (2018).

<sup>32</sup>K. Dileep, L. S. Panchakarla, K. Balasubramanian, U. V. Waghmare, and R. Datta, *J. Appl. Phys.* **109**, 063523 (2011).

<sup>33</sup>P. Torruella, C. Coll, G. Martín, L. López-Conesa, M. Vila, C. Díaz-Guerra, M. Varela, M. L. Ruiz-González, J. Piqueras, F. Peiró, and S. Estradé, *J. Phys. Chem. C* **121**, 24809 (2017).

<sup>34</sup>Z. Guo, F. Ambrosio, and A. Pasquarello, *Appl. Phys. Lett.* **109**, 062903 (2016).

<sup>35</sup>F. Roccaforte, P. Fiorenza, G. Greco, R. Lo Nigro, F. Giannazzo, F. Iucolano, and M. Saggio, *Microelectron. Eng.* **187-188**, 66–77 (2018).

<sup>36</sup>B. Hou, X. Ma, J. Zhu, L. Yang, W. Chen, M. Mi, Q. Zhu, L. Chen, R. Zhang, M. Zhang, X. Zhou, and Y. Hao, *IEEE Electron Device Lett.* **39**, 397–400 (2018).